

Effect of Zn addition on alloy by 0.3, 0.6 and 0.9 wt.% on thermal properties, electrical conductivity and microstructure of eutectic Sn-3.5Ag alloy

Abdullah Muala

Ministry of Education, Dubai, United Arab Emirate

Correspondence: abph83@hotmail.com

Received: (17/10/2021), Accepted: (28/12/2021)

Abstract

In this work, the effects of 0.3, 0.6 and 0.9 wt.% Zn additives on the characteristic of Sn3.5Ag eutectic solder alloy, have been diluted to produce four micro alloys. Effects of 0.3 to 0.9 wt% Zn- additions on phase transformation and electrical resistivity of Sn-3.5Ag eutectic solder alloy have been investigated using Differential Scanning Calorimetry (DSC) and Keithley Source Meter (SMU), respectively. The addition of Zn reduced the melting point of the eutectic Sn-3.5Ag alloy and the pasty range ($T_{\text{end}} - T_{\text{onset}}$) for the *Sn-3.5Ag-0.3Zn*, *Sn-3.5Ag-0.6Zn* and *Sn-3.5Ag-0.9Zn* solder alloys are 8.34, 8.31 and 7.12 °C respectively, decreased from four micro alloys 8.34 °C to 7.12 °C. These results show that the Zn addition is beneficial to decrease the heat of fusion of the *Sn-3.5Ag* solder alloy This improvement is an indication for property enhancing the mechanical properties. It is showing that the solder alloy needs the lowest energy for melting and it is a useful for saving energy also the resistivity increases continuously with Zn content.

Keywords: Zinc Alloys, *Sn-Ag-Zn* Alloy, Thermal Properties, Electrical Resistivity, Mechanical Properties, Microstructure of Eutectic *Sn-3.5Ag*.

Introduction

Zinc alloys have attracted increasing attentions for years, because of their favorable properties zinc alloys are normally used in the form of coatings, castings, rolled sheets, drawn wires, forgings and extrusions for functional and decorative applications **R.M. Shalaby** ^[1].

Increasing considerations on the environmental protection and health hazards of toxic Sn-Pb solders have prompted the development for lead-free solder alternatives in electronic industry. **Hui Yin, Jihua Chen** ^[2]. There is a number of characteristics that plays a vital role in substitution of *Sn-Pb* to *Sn-Ag-Zn* solder such as:

- Environmental issues related to the toxicity and clean castability.
- Owing to their low melting points
- Resistance to atmospheric corrosion
- Close tolerances
- and recyclability

Many of the lead-free alloys are Sn-based alloys. This is attributed to the tin's attractive combination of economic advantages (wide availability, relatively low cost, environmental benignity, a long history of use in solders, and availability of fluxes) and physical properties (low melting temperature, high electrical conductivity and good wettability of common transition metals and alloys). Most *Sn-base* lead-free solders contain only minor amounts of alloying additions **U. Büyük, S. Enginb** ^[3], **Wang XF** ^[4], **Guangang Wanga** ^[5], **Y. M. Leong** ^[6].

Tensile and impact strengths were not influenced by *Zn* addition 0.3 wt.%. However, they deteriorated by further *Zn* addition. A continuous improvement in creep resistance with increase in *Zn* up to 0.9 wt.% was noticed due to the change in phase morphologies and formation of new intermetallic. It was also reported that addition of *Zn* to *Sn-Ag* altered the dendritic microstructure and formed finer eutectic in the matrix owing to its ability to form complex intermetallic compounds. In view to the introduction, this work aims at investigating the influence of *Zn* micro

inclusions, i.e., 0.3, 0.6 and 0.9 wt.% on the microstructure, grain size and mechanical behavior of *Sn-Ag* alloy.

Experimental Procedures

Materials and Specimens Preparation

The starting materials for this research are *Sn-3.5Ag-xZn* ($x = 0, 0.3, 0.6, 0.9$ wt%) were prepared by melting pure tin, silver, zinc with purities of 99.99 % supplied. The experimental weighted compositions of the prepared alloys are shown in Table (1). These samples were melted in a high frequency induction furnace **NABER L 59/SP**. Appropriate quantities of pure elements were weighted and melting them in tube test at 355°C for 2 hours. Subsequent ice quenching to prevent atomic diffusion. The specimens were polished conventionally using decreasing grades of silicon carbide paper and cleaned by acetone. The cast ingots obtained were cold rolled drawn to wire samples of 0.69 mm diameter and 100 mm length. The samples were divided into two groups. For the first group, annealing at 140°C has been carried out for 2 hours in furnace **Heraeus D-6450 Hanu** with temperature-controlled ± 1 °C and then slowly cooled to room temperature with a cooling rate 0.606 °C/min to obtain samples containing the fully precipitated phases and avoids inhomogeneity structure. The second group stay without annealing.

Table (1): Chemical compositions of manufactured alloys (wt. %).

Sample	Alloys	Sn	Ag	Zn
A	<i>Sn-3.5Ag</i>	96.5	3.5	0.0
B	<i>Sn-3.5Ag-0.3Zn</i>	96.2	3.5	0.3
C	<i>Sn-3.5Ag-0.6Zn</i>	95.9	3.5	0.6
D	<i>Sn-3.5Ag-0.9Zn</i>	95.6	3.5	0.9

Thermal Analysis by Differential Scanning Calorimetry:

The basic principle underlying DSC technique is that when a sample undergoes a physical transformation such as a phase transition, heat will need to flow to it than to the reference (typically an empty sample pan) to maintain both at the same temperature. Whether more or less heat must

flow to the sample depends on whether the process is exothermic or endothermic. As a solid sample melts to a liquid, it will require more heat flowing to the sample to increase its temperature. At the same rate as the reference **K. KV, A** ^[7]. This is due to the absorption of heat by the sample as it undergoes the endothermic phase transition from solid to liquid. Likewise, as the sample undergoes exothermic processes. (Such as crystallization) less heat is required to raise the sample temperature. By observing the difference in heat flow between the sample and reference, DSC can measure the amount of heat absorbed or released during such transition **Muala, Abdullah** ^[8].

In a heat flux DSC, the temperature difference between sample and reference sample is recorded as a direct measure of the difference in the heat flow rates to the sample and the reference sample as shown in Figure (1-a). The heat flow rate difference is assigned by calorimetric calibration **Zhou Yiyuan** ^[9], **On Jun Zhao** ^[10] **Luyao Jiang** ^[11].

The thermal properties of the samples were tested using the technique of DSC (NETZSCHSAT 449 F3 Jupiter) as shown in Figure (1-b). The samples of approximate weight of 0.9 mg were heated from 20 to 300 °C with a constant rate of 5.0 °C/min.

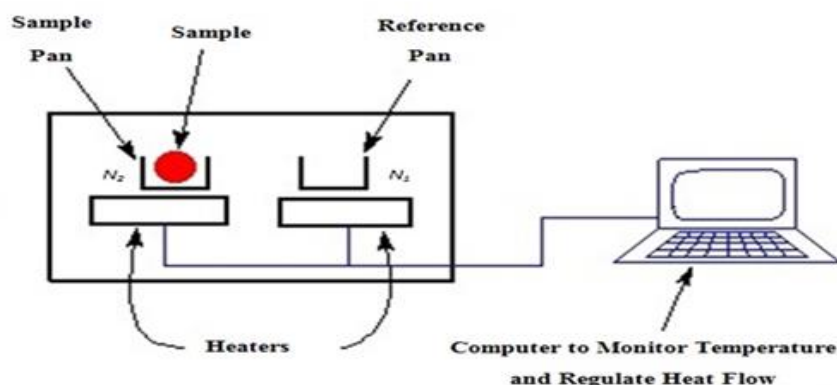


Figure (1-a): Diagram of a specimen geometry, T. Gancarz ^[12], G. Klančnik ^[13].



Figure (1-b): DSC device.

Electrical Resistivity Measurements

In the present work, the electrical resistivity measurements for before and after annealing samples at room temperature using the **Keithley 2004 Source Meter (SMU)** **T. Nakata** ^[14], **MM Hoseini-Athara** ^[15] as shown in Figure (1-c).



Figure (1-c): Keithley 2004 Source Meter device.

Structure Investigation by X-Ray Technique

X-Ray Diffraction in order to investigate and follow the variation of microstructure before and after annealing **Tarek El-Ashram**^[16], Phase identification of the alloy samples is carried out by x-ray diffraction using **XD-2** Powder x-ray Diffractometer with $CuK\alpha$ radiation with a wavelength of 1.54056 \AA at 40 kV and 20 mA radiation with diffraction angle 2θ from 5° to 75° . This technique has been used for measuring the lattice parameter, size of crystalline unit cell. The **X-ray** diffraction pattern of a pure substance is therefore like a fingerprint of the substance.

Results and discussion

The thermal behavior, electrical resistivity and variation of microstructure measurements have been widely used as a of the selected solder alloys results measurements. Done discussed and compared the results of thermal analysis of solder alloys as a function of *Zn* additions on the eutectic alloy *Sn-3.5Ag* in the range of 0.3-0.9 wt.%. Thermal analysis includes discussion of DSC curve, estimating the melting point, comparing the results of selected alloys and other alloys, measuring the pasty range and calculating the heat of fusion for tested solder alloys. Also, in this study discussed and compared the results of the electrical resistivity measurements for before and after annealing samples at room temperature. Also, in this study use X-ray diffraction pattern gives results for the variation of the microstructure for the solder alloys. The objective is to reveal both the internal phases within solder matrix and the effect of separate additions of small amount from 0.3 to 0.9 wt.% of *Zn* on the eutectic alloy *Sn-3.5Ag* microstructure homogeneity.

Thermal Analysis

In soldering process, the melting point of the solder determine the maximum operating temperature of the system and the minimum processing temperature its component must survive. Due to the packaging density of electronic components in the last years, melting point, pasty range and heat of fusion are considered very important thermal properties in evaluation reliability of electronic components. To determine the effect of *Zn* additions on the thermal properties and other possible thermal reaction of the eutectic alloy *Sn-3.5Ag* in the range of 0.3-0.9 wt.%, samples alloys were analyzed by using differential scanning calorimetry has been carried out over the temperature range from 20 to 300 °C. The results of the analyzes as shown in Figures (2 a, b, c) and Figures (3 d, e, f). It indicates that there is not any phase transition before melting which reflect the stability of these alloys with temperature.

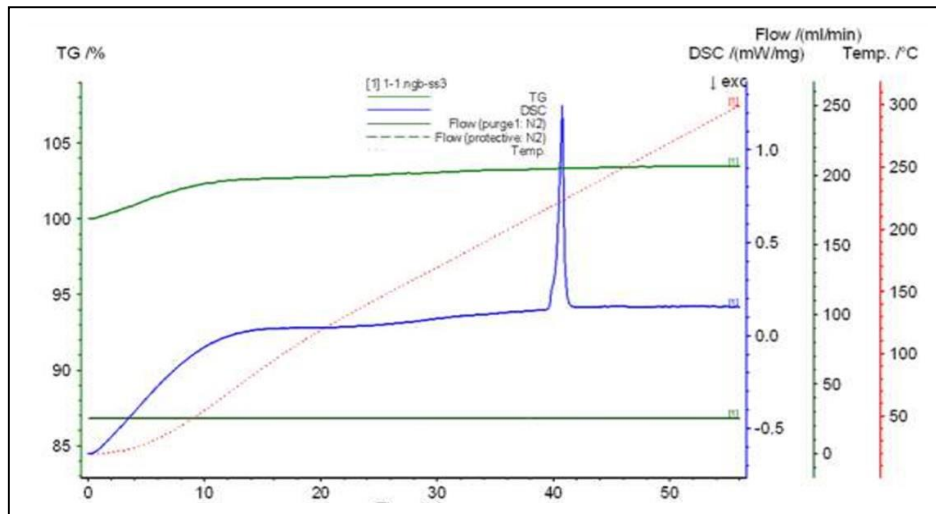


Figure (2-a): Variation of thermal energy flow with time for *B* alloy.

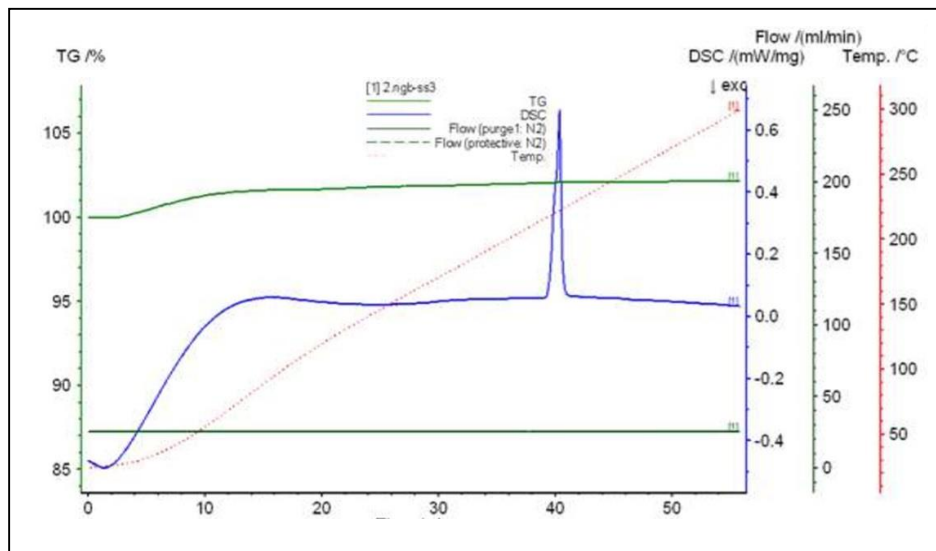


Figure (2-b): Variation of thermal energy flow with time for *C* alloy.

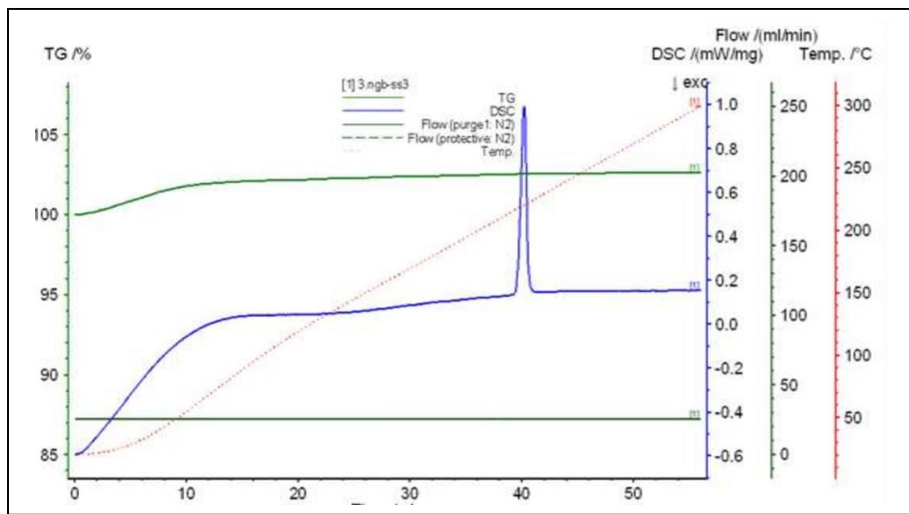


Figure (2-c): Variation of thermal energy flow with time for D alloy.

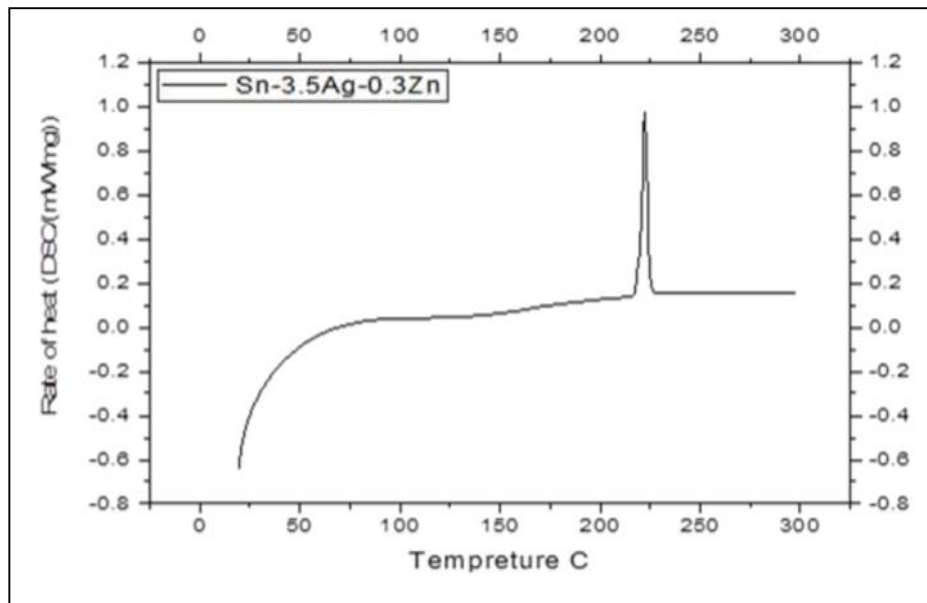


Figure (3-a): DSC curves for A alloy.

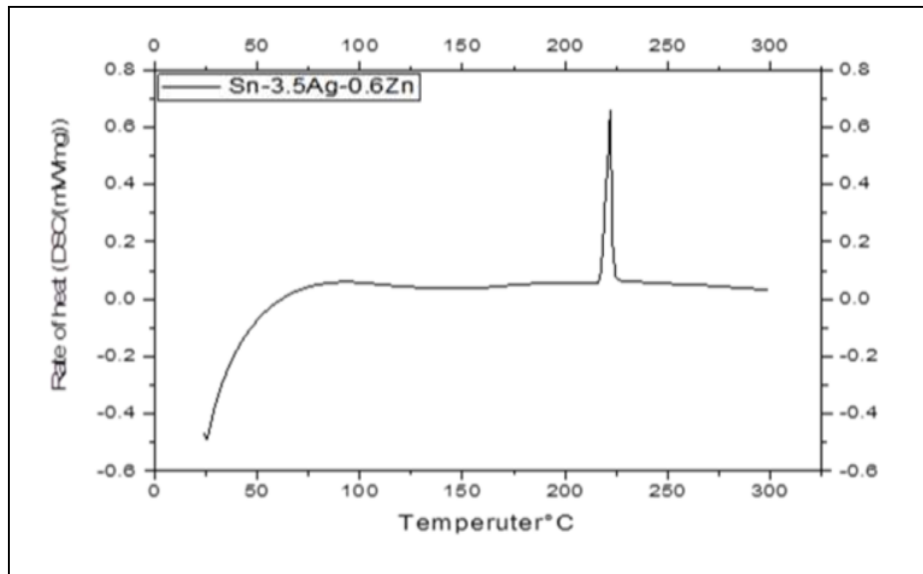


Figure (3-b): DSC curves for *C* alloy.

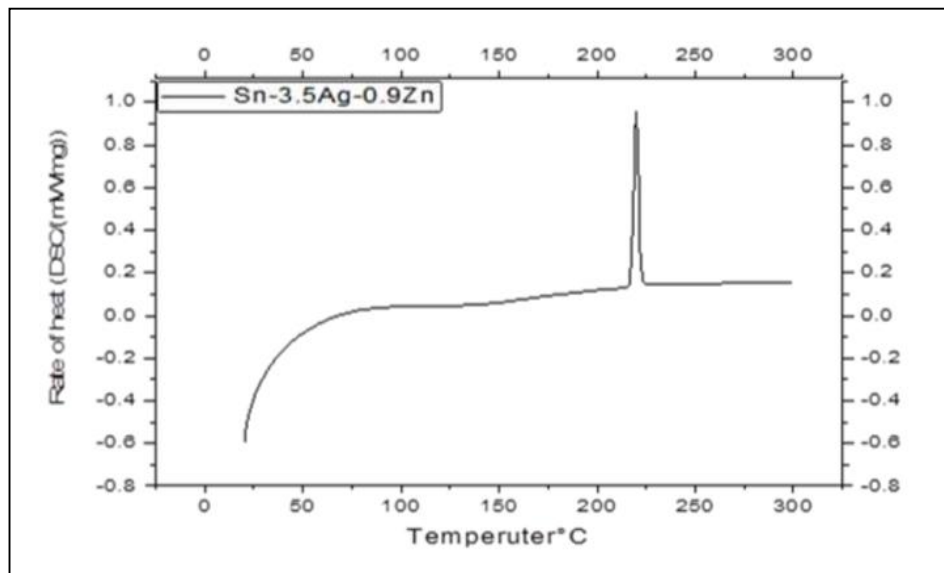


Figure (3-c): DSC curves for *D* alloy.

The DSC results are summarized in Table (2). As a small amount of Zn element was added, the eutectic melting point of Sn-3.5Ag changes significantly. The melting point alloys (Tonset) 217.48, 216.24, and 216.29°C for the Sn-3.5Ag-0.3Zn, Sn-3.5Ag-0.6Zn and Sn-3.5Ag-0.9Zn respectively, as compared with 220.4 °C for Sn-3.5Ag eutectic alloy. The melting point of the solder alloy Sn-3.5Ag reported by K. KV, A. SR [7]. The addition of Zn reduced the melting point of the eutectic Sn-3.5Ag alloy.

Table (2): Comparison between solidus temperature (Tonset), liquidus temperature (Tend), pasty rang, melting point and heat of fusion (ΔH) for the various solder alloys

Compositions	Tonset (°C)	Tend (°C)	Pasty Range (°C)	Melting Point(°C)	ΔH (J/g)
A	220.40	227.80	7.40	220.40	151.000
B	217.48	225.82	8.34	217.48	85.367
C	2016.24	224.55	8.31	2016.24	76.548
D	2016.29	223.41	7.12	2016.29	79.617

The pasty range value, which is the difference between the (T_{end}) and (T_{onset}) temperatures is very important in electronic soldering and other industrial applications. We found that the measured pasty range ($T_{end} - T_{onset}$) for the B, C and D solder alloys are 8.34, 8.31 and 7.12 °C respectively, decreased from 8.34 °C to 7.12°C. The B and C solder alloys are higher than 7.4 °C for eutectic A alloy and D solder alloy is slightly lower than 7.4 °C for eutectic A alloy. The pasty range of the solder alloy A reported by:

$$\Delta H = K_H A_H / m_H, \quad (1)$$

where K_H is the calibration coefficient depending on the shape of a crucible and regarded as a constant in the DSC system, m_H is the mass of a sample and A_H is the area under the curve peak. The calibration coefficient K_H of the DSC instrument is obtained as 2.64, K. KV, A. SR [7].

The DSC result of the various solder alloys shows that the heats of fusion **Muala Abdullah** ^[8], **G. Klančnik** ^[13] G. Klančnik ΔH , for the *C*, Sn-3.5Ag-0.6Zn and *D* solder alloys are 85.367, 76.548 and 79.617 J/g, respectively. The heat of fusion of the solder alloy *A* is 151.0 J/g. The heat of fusion of the solder alloy *A* reported by. The results show the addition of *Zn* to the eutectic *A* alloy decreased the heat of fusion, showing that the *Zn* addition is beneficial to decrease the heat of fusion of the *A* solder alloy. It is showing that the *C* solder alloy needs the lowest energy for melting and is a useful material for saving energy.

Electrical Resistivity Measurements

In most microelectronic applications, the resistivity of the solder interconnect should be so low that its exact value does not affect the functionality of the circuit **Rasim Ozdemir** ^[17]. Table (3) summarizes the values of the room temperature resistivity of *A*, *B*, *C* and *D* alloys before and after annealing. It shows that, the resistivity increases continuously with *Zn* content to its maximum value (17.64 $\mu\Omega\cdot\text{cm}$) at *D* before annealing alloy.

This increase can be attributed to increase existence in scattering centers for conduction electrons, which seem as if small precipitations of *Zn*. All before annealing alloys exhibit higher values of resistivity than after annealing alloys. This increase can be attributed to the presence of vacancies due to directionally solidified process while the annealing process is softened and remove stress. This result is in well agreement with a previous study **Jie Tang** ^[18].

Table (3): Resistivity of alloys before and after annealing.

Alloy	Resistivity of samples before annealing ($\mu\Omega\cdot\text{cm}$)	Resistivity of samples after annealing) $\mu\Omega\cdot\text{cm}$(
<i>A</i>	16.77	12.36
<i>B</i>	16.91	12.77
<i>C</i>	17.13	14.31
<i>D</i>	17.64	5.14

Structural Analysis

X-Ray Diffraction Analysis, the x-ray diffraction is a common characterization technique, which is used to determine phases that found in the metal. To identify the effect of Zn additions on the microstructure of the eutectic alloy Sn-3.5Ag in the range of 0.3-0.9 wt.%, samples alloy was investigated using (XRD) technique before annealing (as received) and after annealing for two hours at 140 °C. The measurements of the annealed samples have been performed after slow cooling of samples to room temperature with (about 0.606 °C/min). Lattice constants were calculated of Sn-3.5Ag, Sn-3.5Ag-0.3Zn, Sn-3.5Ag-0.6Zn and Sn-3.5Ag-0.9Zn alloys before and after annealing. Table (5) represent value of lattice parameters and the variation of **axial ratio** (c/a) with different compositions. It is found that the axial ratio increases to maximum value about 0.54782 at 0.6 wt.% Zn before annealing. X-Ray analysis of Sn-3.5Ag, Sn-3.5Ag-0.3Zn, Sn-3.5Ag-0.6Zn and Sn-3.5Ag-0.9Zn alloys before and after annealing show in Figures (4 a, b, c, d, e, f, g and h).

Table (4): Values of lattice parameters and the variation of axial ratio.

Metal	Sn		
	a (Å)	b (Å)	c/a
Sn-3.5Ag Before annealing	5.79275	3.15967	0.54545
Sn-3.5Ag After annealing	5.79838	3.16889	0.54523
Sn-3.5Ag-0.3Zn Before annealing	5.81205	3.16889	0.54523
Sn-3.5Ag-0.3Zn After annealing	5.80175	3.16464	0.54546
Sn-3.5Ag-0.6Zn Before annealing	5.79679	3.17562	0.54782
Sn-3.5Ag-0.6Zn After annealing	5.80816	3.17174	0.54608
Sn-3.5Ag-0.9Zn Before annealing	5.78680	3.16107	0.54626
Sn-3.5Ag-0.9Zn After annealing	5.98185	3.16616	0.52929

Phase diagram of Sn–Ag–Zn ternary alloy is given in Figure (5), **T. Nakata** ^[14]. It follows that β -Sn, AgZn and Ag₃Sn phases will separate out in the slowly cooled solder and eutectic microstructure consist of the mixture of ζ -AgZn and Ag₃Sn IMCs in the matrix of β -Sn ^[14]. In present work, the X-ray diffraction patterns for Sn-3.5Ag, Sn-3.5Ag-0.3Zn, Sn-

3.5Ag-0.6Zn and Sn-3.5Ag-0.9Zn alloys before and after annealing were found matrix of β -Sn and Ag₃Sn phases as shown in Figures (4 a, b, c, d, e, f, g and h).

AgZn phase in the matrix of β -Sn could not be found with the X-ray diffraction patterns. There is not any evidence to show the microstructure of directionally solidified Sn-3.5wt % Ag-(0.3-0.9wt.%) Zn alloys also consists of AgZn phase in the Sn-rich matrix (β -Sn phase) in present work which agrees with other work **U. T. Nakata** ^[14]. This discrepancy is probably due to the non-zero solubility of zinc in the binary Ag-Sn intermediate phases that we have revealed.

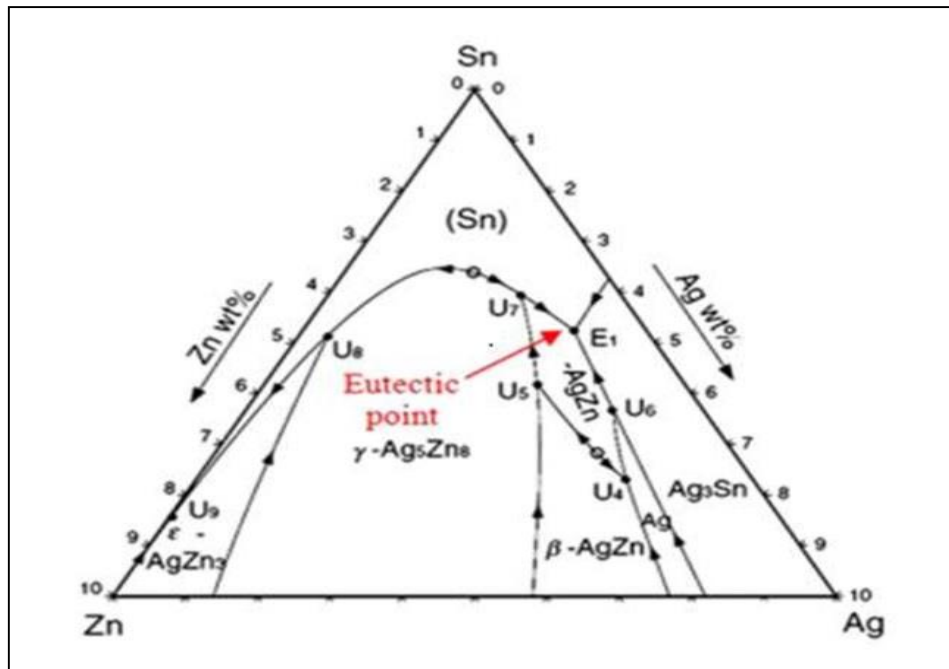


Figure (4): The Sn-Ag-Zn ternary phase diagram ^[3].

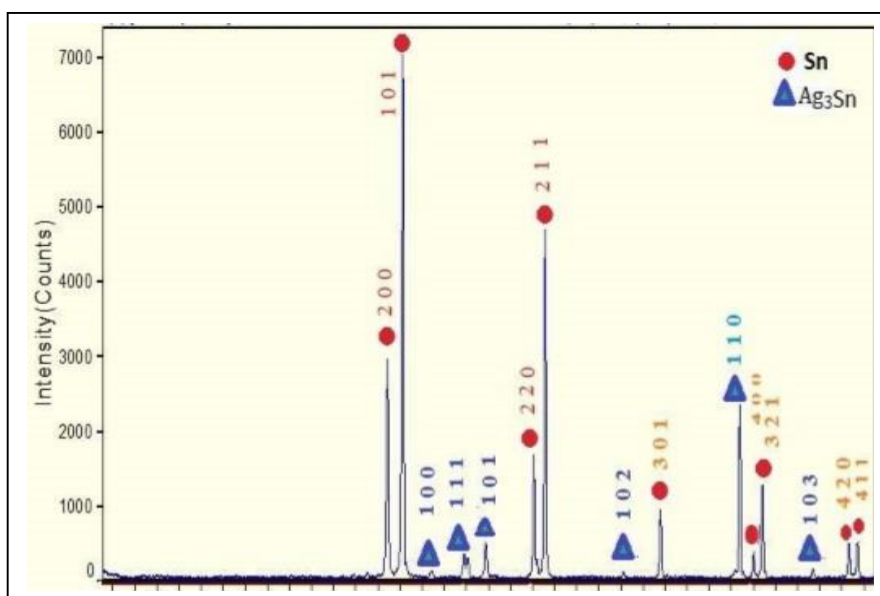
 2θ

Figure (5-a): X-Ray analysis of A alloy before annealing (as received).

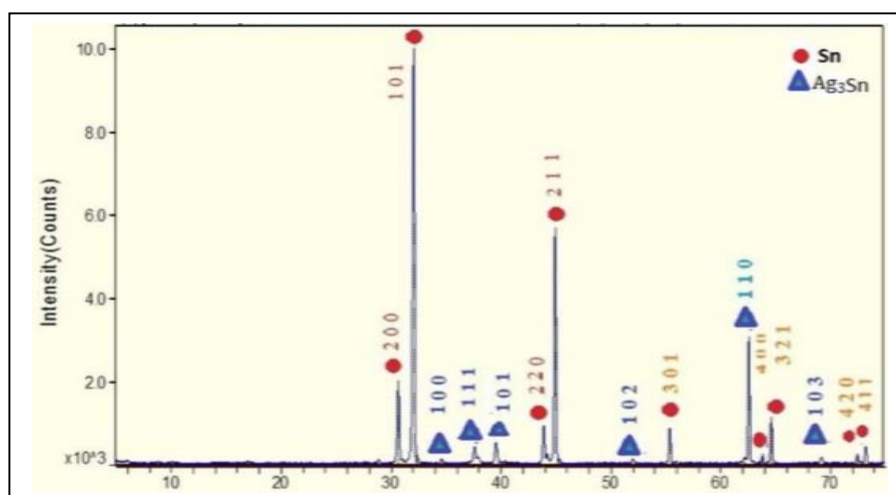
 2θ

Figure (5-b): X-Ray analysis of A alloy after annealing for 2h at (140 °C).

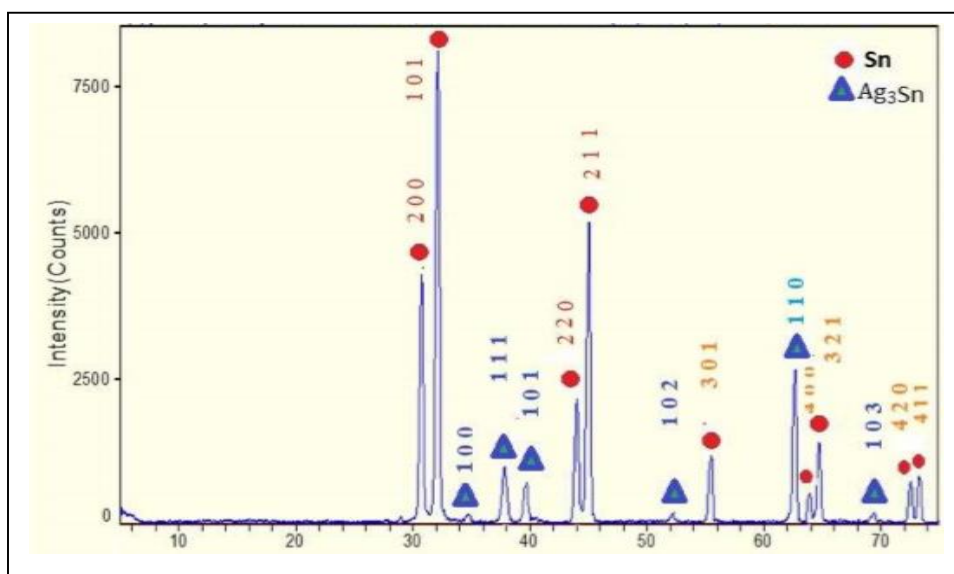
 2θ

Figure (5 - c): X-Ray analysis of *B* alloy before annealing (as received).

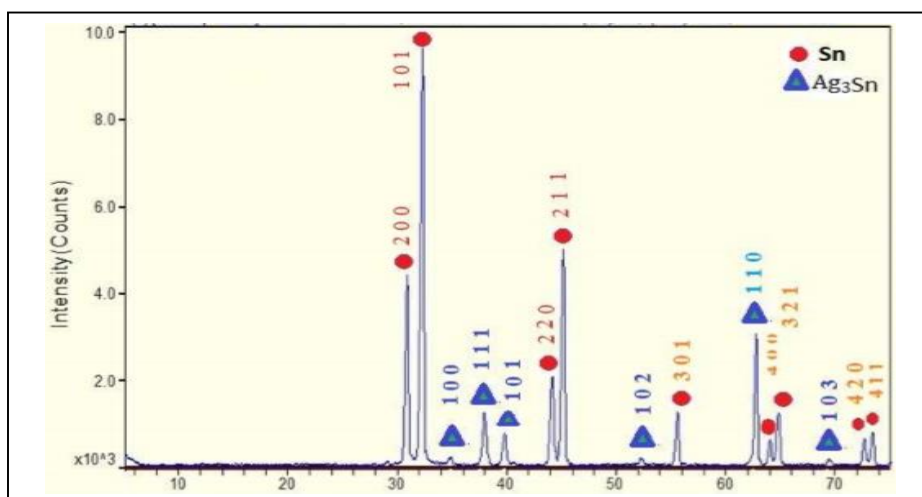
 2θ

Fig (5-d): X-Ray analysis of *B* alloy after annealing for 2h at (140 °C).

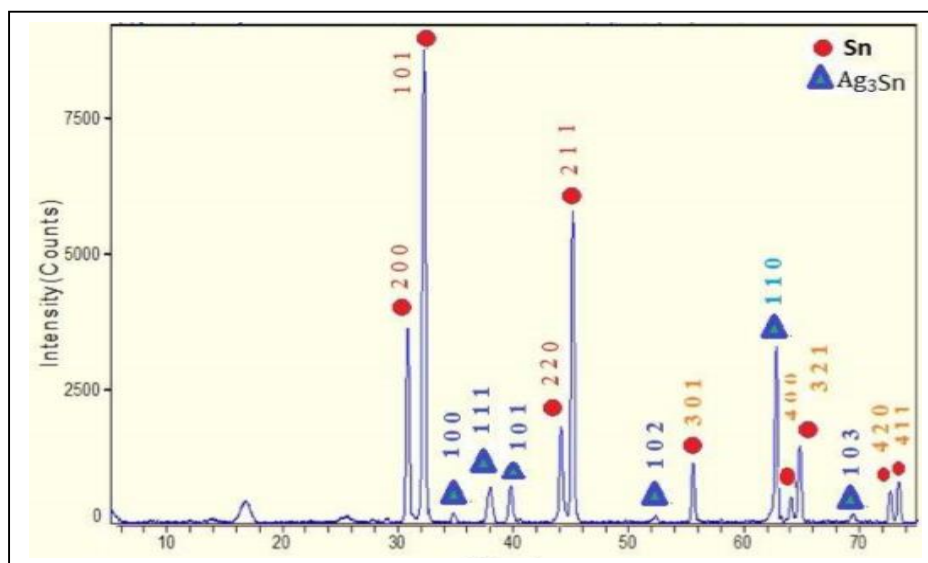
 2θ

Figure (5-e): X-Ray analysis of C alloy before annealing (as received).

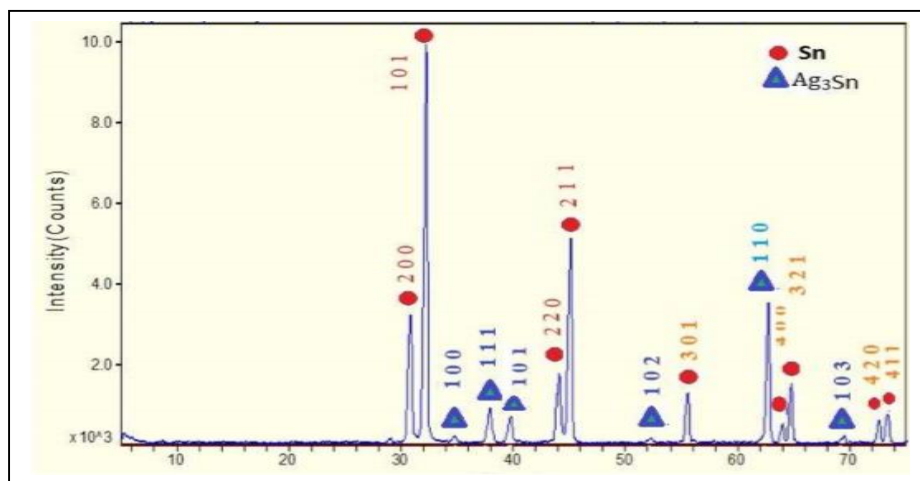
 2θ

Figure (5-f): X-Ray analysis of C alloy after annealing for 2h at (140 °C).

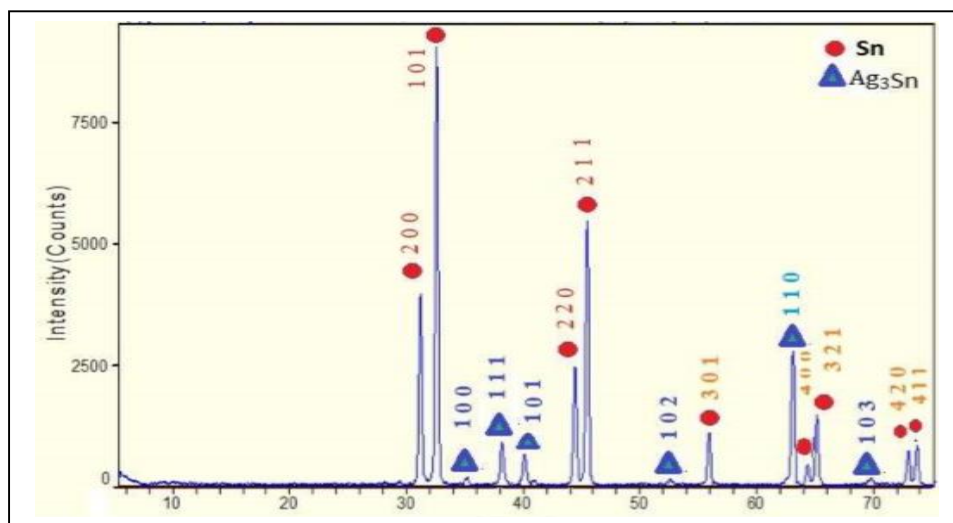
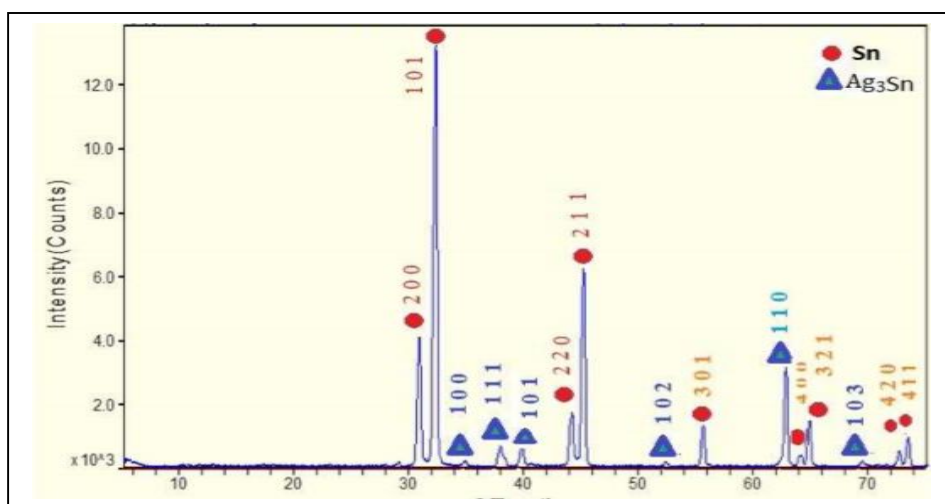
 2θ

Figure (5-g): X-Ray analysis of *D* alloy before annealing (as received).

 2θ

Figure(5-h): X-Ray analysis of *D* alloy after annealing for 2h at (140 °C).

The average crystallite size, D , is given by the analysis of XRD pattern and by using the following Scherrer, **T. Nakata** ^[14].

$$D = K \cdot \lambda / \beta \cdot \cos \theta, \quad (2)$$

where λ is the X-ray wavelength, β is the peak width of the diffraction peak profile at half maximum height resulting from small crystallite size in radians and K is a constant related to crystallite shape, normally taken as 0.9 and θ is the angle of diffraction.

The variations of crystallite size have been calculated and plotted with Zn content as can see Fig. (5 a, b), respectively. The results show the addition of Zn to the eutectic $Sn-3.5Ag$ alloy decreased the crystallite size. The results show that the minimum value of crystallite size $\beta-Sn$ phases was observed for $Sn-3.5Ag-0.6Zn$ after annealing and $Sn-3.5Ag-0.3Zn$ before annealing alloys are 2494.433, 2504.033 nm respectively and the minimum value of crystallite size Ag_3Sn phases was observed for $Sn-3.5Ag-0.3Zn$ before annealing alloy is 2078.7836 nm.

This result is in well agreement with a previous study **Guangang Wanga** ^[5], **Y. M. Leong** ^[6]. So, the small addition of Zn in $Sn-Ag$ solder can suppress the formation of $\beta-Sn$ even at such quenched and thus uniform and refined microstructure can be obtained in it. These decreases in crystallite size may be causes decrease the melting point for the alloys with Zn content as evident with the work of Peters et al **Tarek El-Ashram** ^[16], in which the melting point of metals and alloys decreases as the crystalline size decreases.

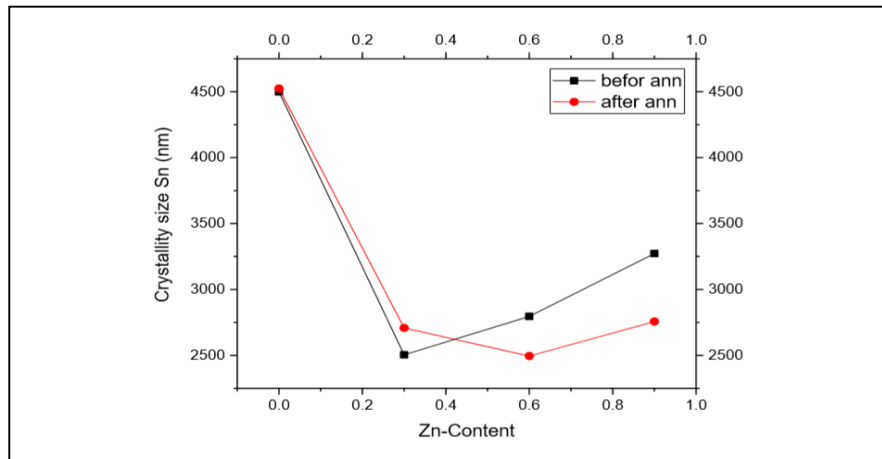


Figure (6-a): Variation of crystallite size β -Sn phases with the zinc content in the system.

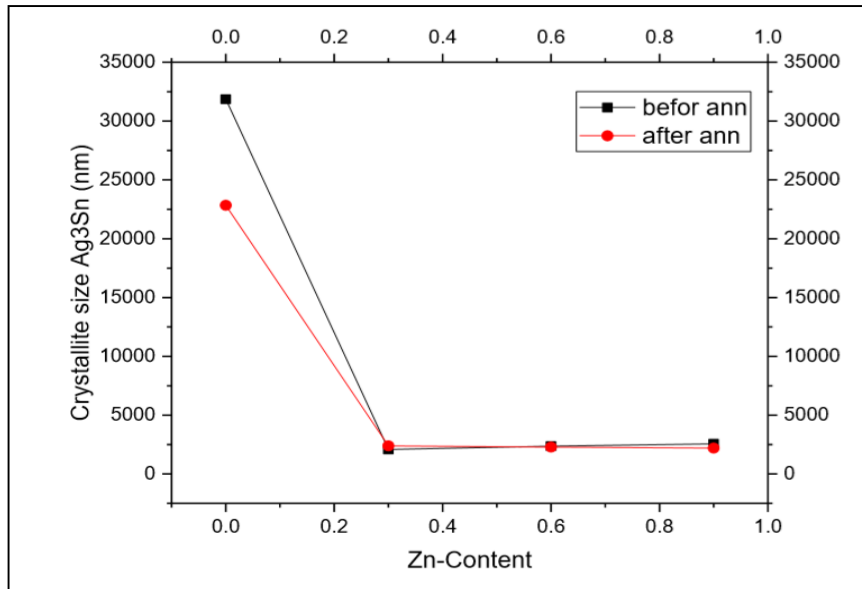


Figure (6-b): Variation of crystallite size Ag_3Sn phases with the zinc content in the system.

Conclusions

In this study, the effects of a third element, i.e., *Zn* in the range of 0.3-0.9wt.%, on thermal properties, electrical resistivity, microstructure of the binary *Sn-3.5Ag* eutectic system lead-free solder alloy were investigated and analyzed. The results are summarized as follows:

1. The addition of *Zn* reduced the melting point of the eutectic *Sn-3.5Ag* alloy proved by thermodynamic calculations and phase assemblage diagrams.
2. The sequence of the pasty range for the various solders are: *Sn 3.5Ag-0.3Zn* > *Sn-3.5Ag-0.6Zn* > *Sn-3.5Ag* > *Sn-3.5Ag-0.9Zn*.
3. The addition of *Zn* to the eutectic *Sn-3.5Ag* alloy decreased the heat of fusion, showing that the *Zn* addition is beneficial to decrease the heat of fusion of the *Sn-3.5Ag* solder alloy. It is showing that the *Sn-3.5Ag-0.6Zn* solder alloy needs the lowest energy for melting and is a useful material for saving energy. From the results obtained from all examined specimens, addition of 0.6 wt.% *Zn* produce optimum mechanical properties at ambient temperature.
4. The addition of *Zn* to the eutectic *Sn-3.5Ag* alloy increased the resistivity. All after annealing alloys exhibit lower values of resistivity than before annealing alloys.
5. The X-ray diffraction patterns for *Sn-3.5wt.% Ag-(0.3-0.9wt.%) Zn* alloys before and after annealing were found matrix of β -*Sn* and Ag_3Sn phases.
6. The addition of 0.3 and 0.9 wt.% *Zn* to the starting alloy transformed the large dendrites into fine equiaxed grains and decreased the crystallite size. When 0.9 wt.% *Zn* was added, coarse equiaxed grains originated.

References

- [1] Shalaby, R.M. (2010). *Effect of rapid solidification on mechanical properties of a lead-free Sn-3.5Ag solder*. *Journal of Alloys and Compounds*. 113-117.

- [2] Hui Yin, Jihua Chen, Hongge Yan, Weijun Xia, Bin Su, Wensen Huang, Xiu. (2021). *Effects of Zn addition on precipitation behavior and mechanical properties of Mg-5Ga alloy*. Volume 291, 15 May 2021, 129495.
- [3] Büyük, U. Engin, S. Kaya, H. & Maraşlıc. N. (2010). *Effect of solidification parameters on the microstructure of Sn-3.7Ag-0.9Zn solder*. Published by Elsevier Inc. *Materials Characterization* 61. 1260 – 1267.
- [4] Wang, XF. Guo, MX. Cao, LY. Luo, JR. Zhang, JS. Zhuang, LZ. (2015). *Effect of heating rate on mechanical property, microstructure and texture evolution of Al-Mg-Si-Cu alloy during solution treatment*. *Mater Sci Eng A* 621. 8–17 .
- [5] Guangang Wang, Guangsheng Huang, Xiang Chen, Qianyan Deng, Aitao Tang. (2017). *Effects of Zn addition on the mechanical properties and texture of extruded Mg-Zn-Ca-Ce magnesium alloy sheets*. *solder material, Materials Science and Engineering*. 705. 29 September 2017. 46-54.
- [6] Leong, Y. M. & Haseeb, A.S.M.A. (2012). *Soldering and interfacial characteristics of Sn-3.5Ag solder containing zinc nanoparticles*. 35th International Electronic Manufacturing Technology Conference. 25-40.
- [7] K. KV, A. SR, Y. PR, P. RY, and B. VU. (2014). *Differential Scanning Calorimetry: A Review*. *Journal of Pharmaceutical Analysis*.
- [8] Mulla`a, Abdullah Tayseer. (2017). *Thermal Analysis and Creep Curve for Some Sn-Ag-Cu Compositions*. Al-Hussein Bin Talal University. 3. 5- 12.
- [9] Zhou Yiyuan, Fu Penghuai, Peng Liming, Wang Dan, Wang Yingxin, Hu Bin, cLiu, Ming Anil K, Sachdev, Ding, Wenjiang. (2019). *Precipitation modification in cast Mg-1Nd-1Ce-Zr alloy by Zn addition*. 7(1). March 2019. 113-123.

- [10] On Jun Zhao, Bin Jiang, Yuan Yuan, Aitao Tang, Haoran Sheng, Tianhao Yang, Guangsheng Huang, Dingfei Zhang, Fusheng Pan A. (2020). Influence of Zn addition on the microstructure, tensile properties and work-hardening behavior of Mg-1Gd alloy. *Materials Science and Engineering*. 772. 20 January 2020. 138779.
- [11] Luyao Jiang, BWeijiu Huang, CFei Guo, Yuhe Zhang, Dingfei Zhang, Qingcai Liu A. (2019). Effects of Zn addition on the aging behavior and mechanical properties of Mg single bond8Alsingl bond2Sn wrought alloy. *Materials Science and Engineering*: 752. 3 April. 145-151.
- [12] Gancarz, T. Pstruś. J. (2015). Characteristics of Sn-Zn Cast Alloys with the Addition of Ag and Cu. *Archives of Metallurgy and Materials*. 60(3). 1603-1607.
- [13] Klančnik, G. Medved, J. Mrvar, P. (2010). Differential thermal analysis (DTA) and differential scanning calorimetry (DSC) as a method of material investigation. *RMZ- Materials and Geoenvironment*. 57(1). 127–142.
- [14] Nakata, T. Coinsa, C. Suzawab, Yoshidab, awabeb, amadoa. (2018). Enhancing mechanical properties of rolled Mg-Al-Ca-Mn alloy sheet by Zn addition. *Materials Science and Engineering*. 737. 8 November 2018. 223-229.
- [15] MM Hoseini-Athara, Mahmudia, Prasath Babub, Hedströmb. (2019). Effect of Zn addition on dynamic recrystallization behavior of Mg-2Gd alloy during high-temperature deformation. *Journal of Alloys and Compounds*. 806. 25 October 2019. 1200-1206.
- [16] Tarek El-Ashram, RM Shalaby. (2019). Effect of rapid solidification and small additions of Zn and Bi on the structure and properties of Sn-Cu eutectic alloy. *Journal of Electronic Materials*. 34. 212–215.
- [17] Rasim Ozdemir, Ismail Hakki Karahan. (2016). A Study on the Electrodeposited Cu-Zn Alloy Thin Films. *Metallurgical and Materials Transactions*. 47. 5609–5617.

- [18] Jie Tang, Hui Zhang, Jie Teng, Dingf Fu, Fulin Jiang. (2019). Effect of Zn content on the static softening behavior and kinetics of Al–Zn–Mg–Cu alloys during double-stage hot deformation. *Metallurgical and Materials Transactions*. 47. 5609–5617.